Unsteady flow regimes in a T-shaped micro-mixer: mixing and characteristic frequencies

Alessandro Mariotti,[†] Chiara Galletti,[†,‡] Maria Vittoria Salvetti,[†] and Elisabetta Brunazzi[*,†]

†*Dipartimento di Ingegneria Civile e Industriale, University of Pisa, Pisa, Italy*

‡*corresponding author*

E-mail: chiara.galletti@unipi.it

Phone: +39 050 2217897

Abstract

Experiments and direct numerical simulations are used jointly to study the asymmetric and the symmetric time-periodic regimes occurring in a T-shaped micro mixer for larger Reynolds numbers than those of steady regimes. The first is characterized by a large mixing degree, while the flow in the second regime always exhibits a nearly double mirror symmetry in the mixing channel, which strongly hampers mixing. The characteristic non-dimensional frequency, calculated using the hydraulic diameter of the mixing channel and the bulk velocity, augments with the Reynolds number in both periodic regimes, but a large discontinuity is observed at the transition between the two regimes. A detailed description of the main flow features is given, in order to provide a physical explanation on the Strouhal number variation. The present analysis can be exploited in practice to design active control strategies, e.g. by exciting the flow at the frequencies typical of the asymmetric unsteady regime.

Contents

List of Figures

Introduction

Microfluidic devices are gaining increasing interest in the synthesis of drugs and fine chemicals because they allow an unprecedented control over operating conditions. In particular, the high surface to volume ratio enables a high heat transfer capacity, thus potentially ensuring a fast and efficient temperature control. This may also lead to the possibility to handle highly exothermic reactions without dilution. As a result, higher reaction yield and selectivity can be achieved with respect to the batch processes that are traditionally used. Indeed, the miniaturization of some synthesis routes may provide effective process intensification , which results in economical, environmental and safety benefits[1–3]).

Micro-reactors are composed of micro-channels, with typical dimensions ≤ 1 mm; two or more reactants are fed through inlet branches and then mix in the mixing channel. The flow is laminar due to the tiny dimensions; hence specific methods have to be developed in order to improve the mixing of reactants and thus reaction yields[4 5 6 7 8]. Active enhancing methods are based on external energy sources (e.g., ultrasound, electric field) and the idea behind them is to induce oscillations of the flow field on purpose to improve mixing. These oscillations can be driven, for example, by pulsating inlets, as proposed by Ito and Komori, who employed a small vibrating motor to pulsate the flow entering a Y-shaped mixer.[9] Similarly, Sun and Sie used a dynamic pressure generator to feed with a sinusoidal pressure profile the liquids entering a T-mixer with a divergent channel.[10] Recently, Erkoc et al. investigated numerically the mixing process in a 2D T-jet mixer using a pulsation/modulation of the jets flow rate.[11]

However oscillations of the flow, namely flow instabilities, can be present naturally in the laminar regime even with steady inlet conditions and in absence of any external force, i.e. in passive micro-devices. In particular, for a simple T-mixer, it was observed that the flow may become time-periodic for specific ranges of the mixing channel Reynolds number $Re = \rho U d/\mu$. Here ρ is the density of the fluid, U is the inlet bulk velocity, d is the mixing-channel hydraulic diameter and μ is the fluid dynamic viscosity. In particular, in case of square inlet

sections fed with two water streams with equal flow rates, the flow is steady up to $Re = 220$ but subsequently it becomes time-periodic and eventually chaotic. The steady regimes have been largely characterized in literature and may be classified into: stratified, vortex (steady symmetric) and engulfment (steady asymmetric) regimes[12,13,14,15,16,17,18,19,20]. Then, at $225 \leq Re \leq 320$ the flow exhibits a time-periodic motion with a large degree of asymmetry (periodic asymmetric regime) and, thus, with a large degree of mixing [21]. This can be even 30-50% higher than the one observed in the steady engulfment regime[16].[22] However, with further increasing Re, i.e. at $325 \leq Re \leq 510$, the flow, although still time-periodic, unexpectedly presents a higher level of symmetry with a detrimental effect on the degree of mixing[23] (periodic symmetric regime). Evidences of the time-periodic motions were provided by the numerical simulations of,[16,24,25] and[26] and further supported by experiments of[27,28] and.[23] The effect of channel aspect ratio on the periodic motions was analysed in,[29] while the influence of the liquid mixture properties by.[22] The presence of unsteady regimes was also observed in opposed T-jet mixers with different aspect ratios[30] Some of the previous works tried to characterized the time-scales typical of the above unsteady regimes, in particular in terms of Strouhal number, St, usually defined by using the bulk velocity of the flow and a geometrical characteristic length, as e.g. the mixing channel hydraulic diameter. Besides a significant dispersion of numerical and experimental data, it was observed (see e.g.[29]) that there is a sudden decrease of St when passing from the asymmetric periodic regime to the symmetric one and this is consistent with the completely different dynamics of these two regimes. Within each regime, however, the Strouhal number is not constant; conversely, it monotonically increases with the Reynolds number. This indicates that the characteristic time-scales are related to dynamic features which depend on the Reynolds number.

The present work further investigates the dynamics of the periodic flow regimes which take place naturally in micro-devices, with the aim of shedding light into the characteristic time-scales and of correlating them to flow features and degree of mixing. In particular, the idea is to find which are the most relevant phenomena occurring in the different regimes which

could be used to define a characteristic time-scale independent of the Reynolds number. This can be useful, e.g., to devise strategies for control and optimization of the mixing process.

T-mixer geometry

The mixer has two inlet channels joining in a T-shaped junction and it is sketched in Fig. 1(a), reporting also the adopted reference frame. This geometry is the one also investigated in.[23] The inlet channels present a square cross-section, i.e. $W_i = H = 1$ mm, whereas the outflow channel has an aspect ratio $2:1$, i.e. $W_o = 2H = 2$ mm. Hence, the mixing-channel hydraulic diameter is $d = 4H/3$. This quantity will be used in the following text to define non-dimensional coordinates, i.e. $X = x/d$, $Y = y/d$ and $Z = z/d$. The length of the inlet channels is $L_i = 40$ mm$\approx 30d$, so the flow at the confluence is fully developed.[31] The length of the mixing channel is $L_o = 60$ mm $\approx 45d$ and allows a complete development of the vortical structures.[23,29]

Experimental set-up

The T-mixer model is in polymethylmethacrylate (PMMA) (see Fig. 1(b)) and is made of three layers, which are sealed with two double-sided adhesive films and screws. The top and bottom layers are equipped with fluidic connections and allow optical access. The central layer, with a thickness equal to 1 mm, has a T-shaped cutting through.

The mixer inlets are fed by means of a Gemini 88 syringe pump at equal flow rates with deionized water streams. In order to discern the two flow streams and capture the mixing process, one inlet stream is colored by means of a Ponceau 4R dye (Sigma-Aldrich) using a concentration of $C_0 = 1.9 \cdot 10^{-3}$ M. This concentration was observed to do not alter the fluid properties. After each experimental test, the pump is stopped and then started again to reach the desired flow rate for a new test. This was made to avoid any hysteresis in the mixing process. Moreover, the pump behavior was observed to be perfectly steady; some

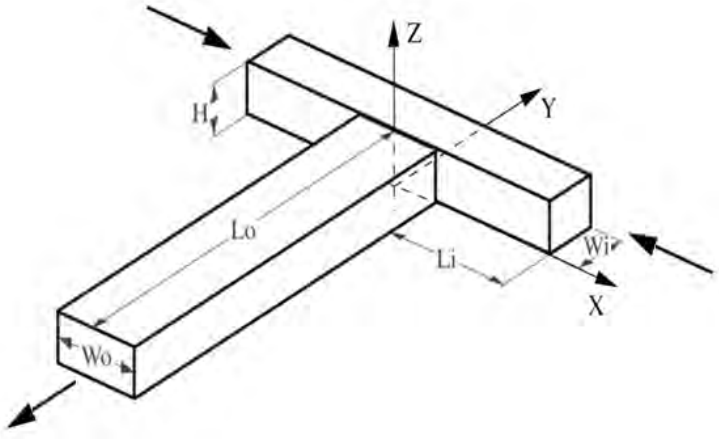

(a)

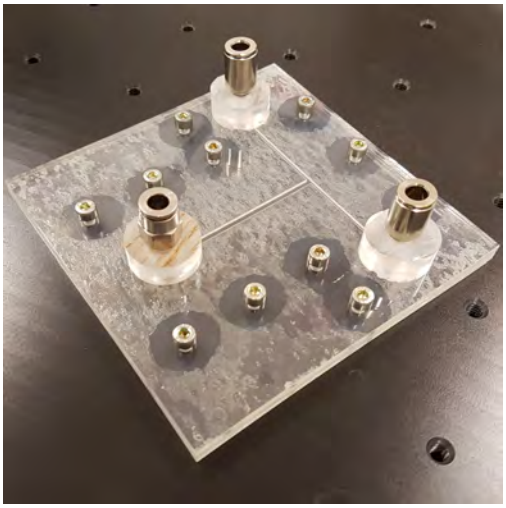

(b)

Figure 1: (a) Geometry of the T-mixer; (b) experimental model.

small pulsations could hardly be observed only for $Re < 20$, thus for much lower flow rates than those used in the present investigation.

The upright microscope Nikon Eclipse 80i with a magnifying lens of 4× was employed to visualize the mixing of the streams. The Optomotive Velociraptor high-speed camera captured the images. The camera resolution is 920 × 2048 pixels with a frame rate equal to 387 frames/s. In front of the camera is mounted a 0.5× lens to collect a region of $1.8d$ × $4d$ in a single image. This arrangement allowed to visualize both T-junction and the mixing-channel initial region. The equivalent length of a pixel is 2.5 μm. More details about the experimental set-up can be found in.[23]

The light emitted from the lamp crosses the fluid and hence the resulting intensity, captured by the camera, depends on the dye concentration. The Lambert-Beer's linear relationship between dye concentration and light absorbance was found to hold by means of preliminary calibration runs in.[23] Thus, normalized depth-averaged dye concentration images can be derived from the light intensity images by using the following equation applied for each (i, j)-th pixel of the images:

$$\frac{ln\left(I_{blank,ij}\right) - ln\left(I_{ij}\right)}{ln\left(I_{blank,ij}\right) - ln\left(I_{max,ij}\right)} = \frac{C_{ij}}{C_0} \tag{1}$$

where, I_{ij} is the instantaneous values of intensity of the light, C_{ij} is the instantaneous values of dye concentration, $I_{blank,ij}$ is the value of light intensity acquired when the mixer is full of only the blank solution and the C_0 is the one when the mixer is full of the C_0 dye solution.

An off-line automatized procedure was developed to post-process the images and thus pixel intensity maps are converted into distributions of normalized depth-averaged dye concentration.[32] The acquisition of the references $I_{blank,ij}$ and $I_{max,ij}$ was necessary for each set of experiments before using the two streams together.

Simulation set-up and numerical methodology

The open-source spectral-element code Nek5000[33] was used to solve the unsteady incompressible Navier-Stokes equations describing the liquid motion. Their non-dimensional form is:

$$\nabla \cdot \mathbf{u} = 0 \tag{2}$$

$$\frac{\partial \mathbf{u}}{\partial \theta} + \mathbf{u} \cdot \nabla \mathbf{u} = -\nabla P + \frac{1}{Re} \nabla^2 \mathbf{u} \tag{3}$$

Here $\partial/\partial\theta$ is the time derivative and P is the modified non-dimensional pressure. The time is normalized using the convective time d/U, the length using hydraulic diameter d of the mixing channel, while the velocities through the bulk velocity U at the inlet. The above equations are coupled with a conservation transport equation for the dye mass fraction ϕ:

$$\frac{\partial \phi}{\partial \theta} + \mathbf{u} \cdot \nabla \phi = \frac{1}{Pe} \nabla^2 \phi, \tag{4}$$

where the Peclet number $Pe = Ud/D$, with D being the molecular diffusivity of the dye.

The numerical set-up is the same as in.[23] A multi-block structured grid having 12250 hexahedral spectral elements is employed for the spatial discretization. The spaces of velocity and pressure are spanned by means of Lagrange polynomial interpolants, which, in each spectral element, are based on tensor-product arrays of Gauss-Lobatto-Legendre (GLL) quadrature points. The polynomial order is $N = 7$ for the velocity and $N - 2 = 5$ for the pressure (P_N/P_{N-2} scheme) resulting, for each component of velocity, in approximately $4 \cdot 10^6$ degrees of freedom. Previous works have indicated that both grid and polynomial order are suitable for this kind of simulations[23,34,35].

For time discretization, a third order backward differential formula (BDF3) is applied. The diffusive terms are handled implicitly, whereas convective terms are treated by means of a third order explicit extrapolation (EXT3). The non-dimensional time-step is $7.0 \cdot 10^{-4}$, ensuring CFL number ≤ 0.3. As for the dye equation, a rather small Schmidt number

should be used to avoid stability issues, i.e. $Sc = \mu/(\rho D) = O(100)$ (see also[26]). This Sc is much lower than the typical values for liquids, i.e. $Sc = O(10^3 \div 10^4)$. Nevertheless, it was demonstrated in[35] that this enhanced diffusion has negligible effects for the investigated region of the T-mixer, i.e. $-0.75 \leq Y \leq -3$, because the residence time is too low to allow molecular diffusion to prevail over transversal convection.

Boundary conditions consist of no-mass-flux and no-slip velocity at the walls, uniform concentration and velocity at the inlets and free outflow conditions at the mixing channel exit.

Uniform dye concentration and non-developed conditions were used to initialize all simulations, to avoid hysteresis issues that may occur especially near flow regime transitions (see e.g.[29,36]). After discarding the initial transient, the total time spanned by a simulation covers more than 20 periodic cycles.[34] In order to compare directly the results of the simulations with the experimental flow visualizations, the depth-averaged dye concentration is calculated from the numerical data.

The mixing degree δ_m between the two streams is estimated for a given mixing channel cross-section Y as [37,38]:

$$\delta_m = 1 - \frac{\sigma_b}{\sigma_{max}} \tag{5}$$

where σ_b is the standard deviation of the volumetric flow, i.e.:

$$\sigma_b^2 = \frac{\int (\phi - \bar{\phi}_b)^2 u_y \, dx \, dz}{\int u_y \, dx \, dz} \tag{6}$$

Here u_y is the y component of the velocity and $\bar{\phi}_b$ is the bulk mass fraction:

$$\bar{\phi}_b = \frac{\int \phi u_y \, dx \, dz}{\int u_y \, dx \, dz} \tag{7}$$

The maximum value of σ_b is denoted here with σ_{max} and is obtained for completely segregated

streams, resulting in:

$$\sigma_{max} = \sqrt{\bar{\phi}_b(1 - \bar{\phi}_b)} \tag{8}$$

Accordingly δ_m is between $\delta_m = 0$, indicating a completely segregated flow, and $\delta_m = 1$, corresponding to a perfectly mixed flow.

Main results

The experimental depth-averaged concentration maps (flow visualizations) shown in Fig. 2 give an overview of the steady and unsteady flow regimes taking place in the T-mixer as a function of the Reynolds numbers Re comprised between 220 and 520. For the unsteady regimes, the shown pictures are just snapshots, i.e. they refer to an arbitrary instant. Videos for all the regimes are provided in the supplementary materials. With increasing the Re number the following regimes are observed: steady asymmetric regime (engulfment regime), unsteady asymmetric regime, unsteady symmetric regime and finally chaotic regime. The qualitative features of the regimes are the same in the whole range of Re within each regime. The transition between the flow regimes is usually very sharp. For instance at $Re = 220$ the flow is steady, whereas at $Re = 225$ a time-periodic motion is present. Similarly, at $Re = 320$ the unsteady flow is asymmetric whereas at $Re = 325$ it is characterized by a large degree of symmetry. Eventually, at $Re = 510$ the flow is almost symmetric, while at 520 the flow is chaotic.

A detailed description of the regimes occurring in the same device was given in.[23] In the present work, we focus on the unsteady periodic regimes, by investigating the flow characteristics and the relevant frequencies, with the aim to further characterize the dynamics and the features that can be exploited to devise strategies to control and improve the mixing process.

In the range $225 \leq Re \leq 320$ the flow exhibits a periodic motion with a high degree of asymmetry in the mixing channel, thus resulting in a large degree of mixing. As described

in,[23] the flow periodicity is strictly linked to the dynamics of 3D vortical structures, which can be briefly summarized as follows: the flow cycle can be thought to start from a configuration which is typical of the steady engulfment regime, in which two counter-rotating vortical structures originate in the recirculation regions near the top walls of the mixer. These structures are not perpendicular to the inlet flow direction, but they are tilted of a certain angle. Moreover, they are convected into the mixing channel, forming two legs for each vortical structure. Due to the tilting, the two legs of each vortex entering in the outflow channel are not equal in terms of intensity, shape, and position. Moving towards the end of the mixing channel, the weakest couple of legs disappears and only two co-rotating vortices survive. During the time cycle the top parts of the vortical structures become closer and their tilting angle increases, until they merge and the top parts, carrying vorticity of different sign, rapidly annihilate, whereas the two stronger legs form a blob of vorticity (i.e. a region of high concentrated vorticity) which is convected in the mixing channel. The signatures of this complex vorticity dynamics can be seen in the predicted depth-averaged dye concentrations reported in Fig. 3 which also provides a quantitative comparison between predictions and experiments at $Re = 280$ for different time instants during a whole characteristic dynamic cycle. The dynamic cycle has a time period τ, corresponding to a Strouhal number $St = d/(U\tau) = 0.218$, calculated using the bulk velocity and the hydraulic diameter of the mixing channel. Since the experimental acquisition frequency rate is 387 Hz, about 11 frames are present at $Re = 280$ for each cycle. The results of 8 significant time instants are reported in Fig. 3, while all the results during 5 cycles can be seen in the attached video. For each time instant, Fig. 3 reports the experimental and predicted depth-averaged dye concentrations (in the middle and right bottom panels) as a function of the X coordinate at two different Y locations in the mixing channel, i.e. $Y = -0.15$ and $Y = -1.30$. Moreover, for the sake of clarity, the numerical distributions of the depth-averaged dye concentration in the mixing channel (left panels) and of the dye concentration in the considered cross-sections (middle and right top panels) are reported. The agreement between the experimental and

numerical results is very good, especially taking into account the fact that the considered flow regime is significantly complex and unsteady. The agreement can be quantified by the coefficient of determination, i.e. R^2, which was estimated by taking all experimental and numerical observations of the depth-averaged dye concentration at different time instants. Very high values were obtained, i.e. $R^2 = 0.967$ and $R^2 = 0.965$ at $Y = -0.15$ and $Y = -1.3$, respectively. The beginning of the cycle is arbitrarily chosen at $t = 0.27\tau$ (Fig. 3(a)), when the flow pattern is close to the one of the steady engulfment regime (compare with Fig. 9(b) in[23] obtained for $Re = 200$), except for the bottom part, in which a signature of the passage of the previous blob of vorticity is still present. The frames from $t = 0.27\tau$ to $t = 0.64\tau$ (Fig. 3(b)) have all similar flow features. The dye distributions in the two cross-sections in the range $t = 0.27 - 0.64\tau$ are similar to the ones of the steady engulfment regime (compare with Figs. 10(a,c) in[23] obtained for $Re = 200$). The two vortical structures at the top of the mixer are really close (see the left panel in Figs. 3(a,b)) and the signature of the two co-rotating stronger vortical legs in the mixing channel can be identified in the dye concentration fields (central and right panels). Both at $Y = -0.15$ and $Y = -1.3$ the two strong legs are clearly detectable and become larger moving downstream in the mixing channel. At $t = 0.73\tau$ (Fig. 3(c)) the two vortical structures start to become closer and to merge, while at $t = 0.82\tau$ (Fig. 3(d)), they merge and their top parts, carrying vorticity of different sign, annihilate whereas a blob of vorticity is formed by the two stronger legs. The two co-rotating stronger vortical legs are really close at $Y = -0.15$ in the mixing channel, while no appreciable effect of the vorticity blob shedding can be seen yet at $Y = -1.3$. The effect of the passage of the vorticity blob at section $Y = -0.15$ is clearly evident at $t = 0.91\tau$ and $t = 1.00\tau$ (Figs. 3(e,f)), while the blob passes at section $Y = -1.3$ at $t = 1.09\tau$ (Fig. 3(g)). The vortex legs present in the channel twist during the passage of the vorticity blob in the mixing channel, with a sudden change in the topology of the dye visualization. In the meanwhile, the top parts of two new structures start to form again entering from the two inlet channels and can be seen at section $Y = -0.15$ in Fig. 3(g) and in both sections

in Fig. 3(h) at $t = 1.18\tau$. Then, the new vortical structures experience the same dynamics, thus beginning a new cycle, as the previously described one.

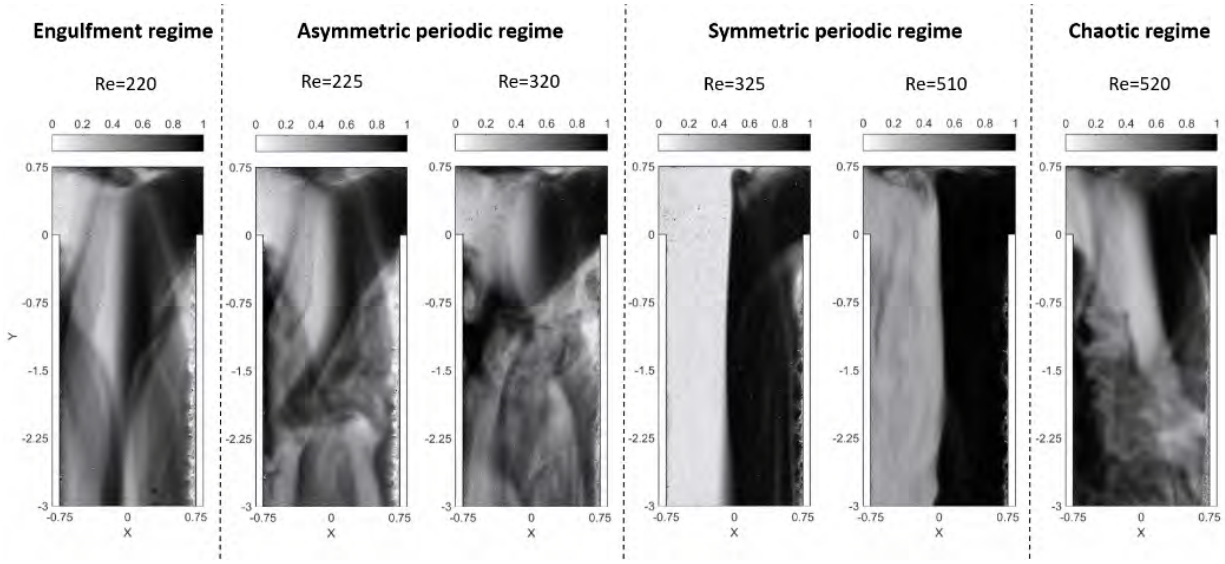

Figure 2: Experimental flow visualization of the different flow regimes occurring in the T-mixer (see also the video attached in the supplementary materials).

The time-behavior of pressure, velocity and dye concentration three-dimensional fields are available from numerical simulations. Hence, the related time-signals can be acquired in suitable locations and analyzed to identify the significant flow frequencies. Our objective is also to derive the frequencies from the depth-averaged concentration field measured in the experiments. To this aim, we wish to ascertain whether the depth-averaged dye concentration signal also contains the characteristic frequencies of the flow dynamics as done by the three-dimensional velocity field. Let us start by analyzing the time signals of velocity recorded in CFD simulations. The time-signal of the x-velocity for $Re = 280$ at $(X, Y, Z) = (0.375, -0.15, 0.375)$ is reported in Fig. 4(b) (Fig. 4(a) shows the position of the probe). The signal clearly indicates a time-periodicity; a negative peak in the x-velocity occurs every time a vorticity blob passes through the mixing channel. The time-signal of the corresponding depth-averaged dye concentration, i.e. at $(X, Y) = (0.375, -0.15)$, is reported in Fig. 4(c). An abrupt increase in the dye concentration takes place when the blob crosses the probe position. For all the different locations considered, the maximum time difference

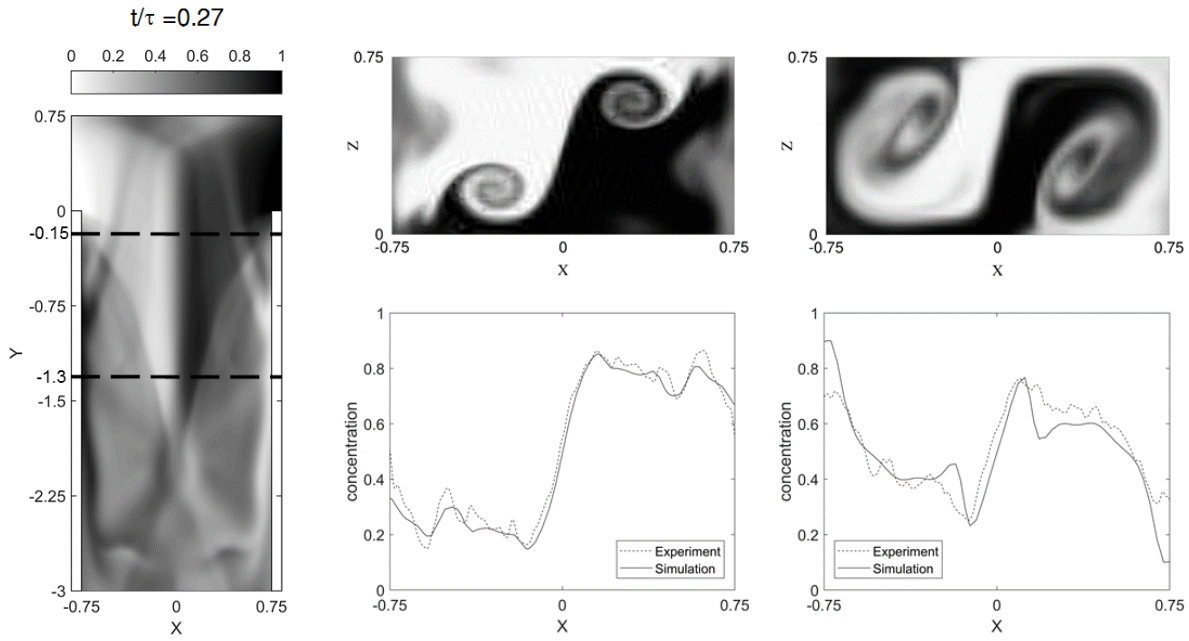
t/τ =0.27
0 0.2 0.4 0.6 0.8 1
0.75
0
-0.15
-0.75
-1.3
-1.5
-2.25
-3
Y
-0.75 0 0.75
X
Z
concentration
Experiment
Simulation

(a)

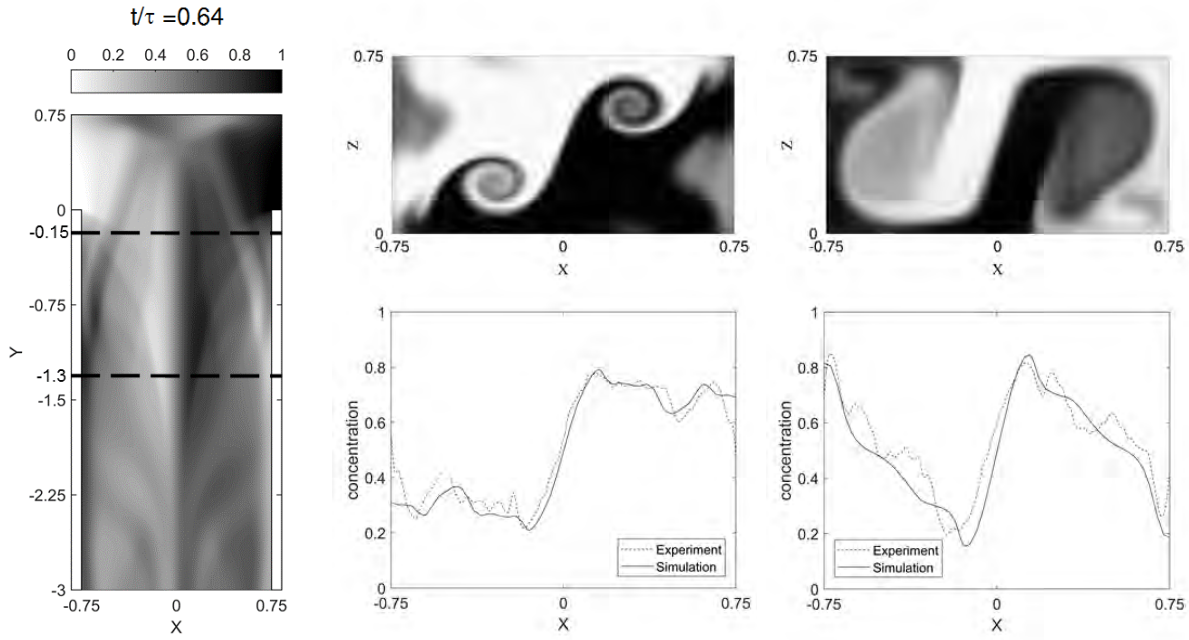
t/τ =0.64
0 0.2 0.4 0.6 0.8 1
0.75
0
-0.15
-0.75
-1.3
-1.5
-2.25
-3
Y
-0.75 0 0.75
X
Z
concentration
Experiment
Simulation

(b)

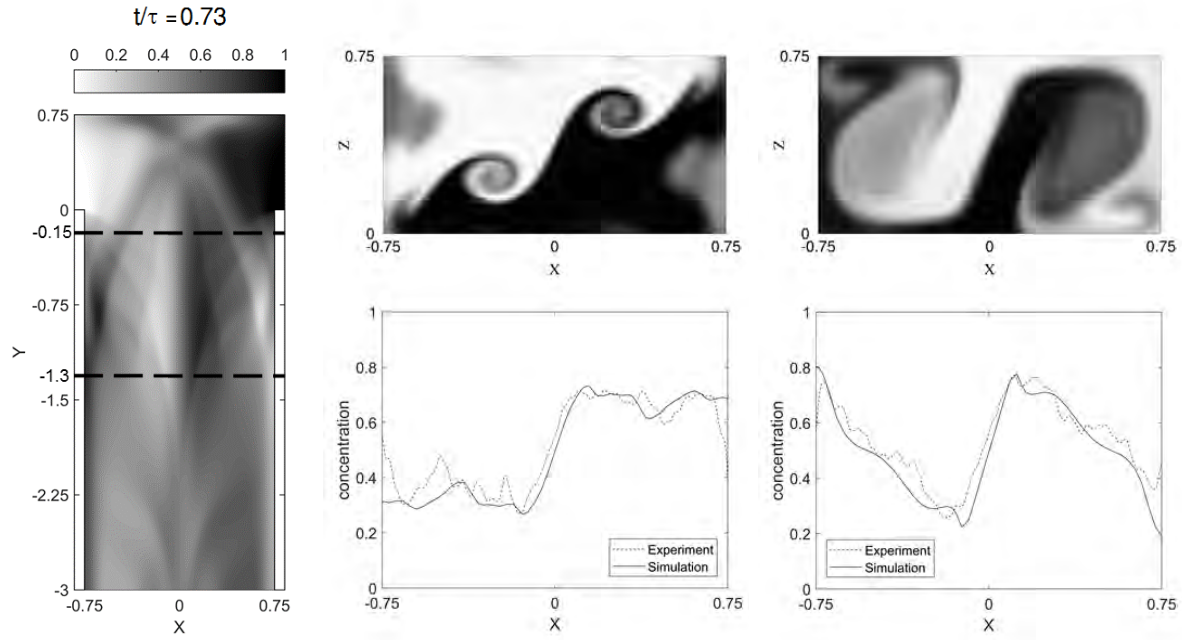
t/τ =0.73
0 0.2 0.4 0.6 0.8 1
0.75
0
-0.15
-0.75
-1.3
-1.5
-2.25
-3
Y
-0.75 0 0.75
X
Z
0.75
0
-0.75 0 0.75
X
concentration
1
0.8
0.6
0.4
0.2
0
Experiment
Simulation

(c)

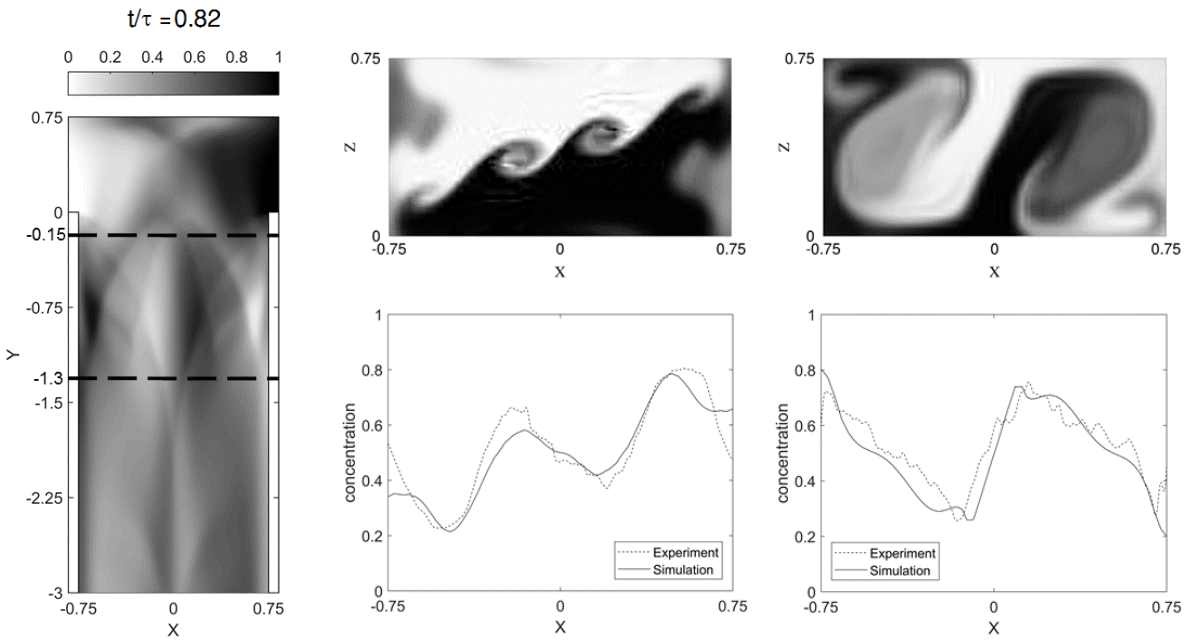
t/τ =0.82
0 0.2 0.4 0.6 0.8 1
0.75
0
-0.15
-0.75
-1.3
-1.5
-2.25
-3
Y
-0.75 0 0.75
X
Z
0.75
0
-0.75 0 0.75
X
concentration
1
0.8
0.6
0.4
0.2
0
Experiment
Simulation

(d)

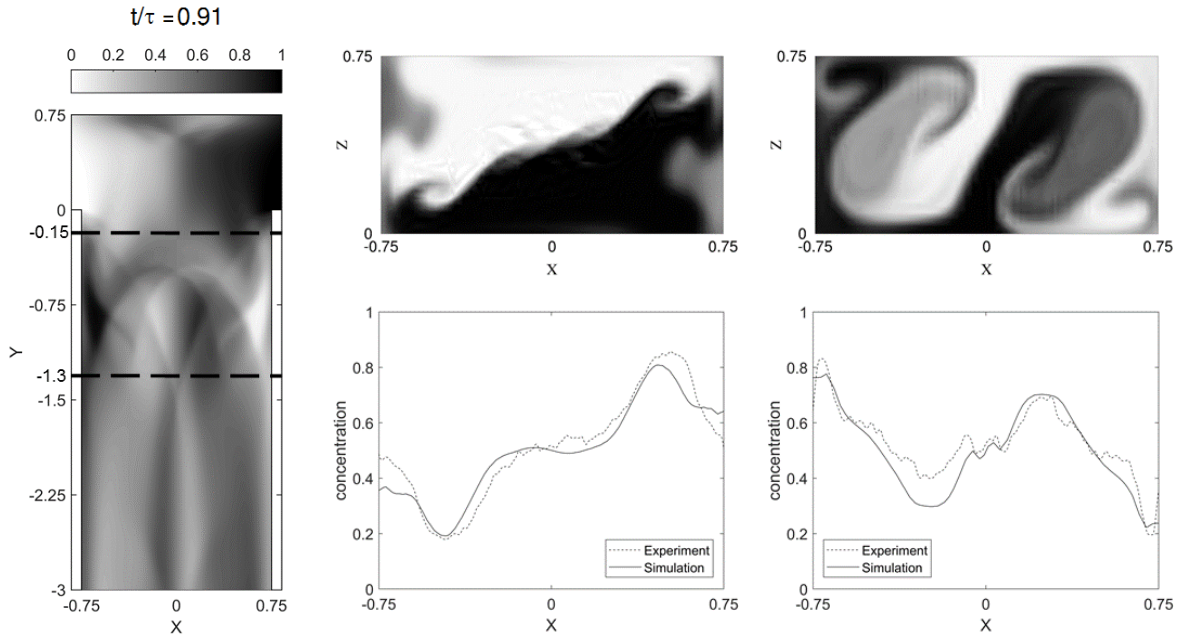
t/τ =0.91
0 0.2 0.4 0.6 0.8 1
0.75
0
-0.15
-0.75
-1.3
-1.5
-2.25
-3
Y
-0.75 0 0.75
X
Z
X
concentration
Experiment
Simulation

(e)

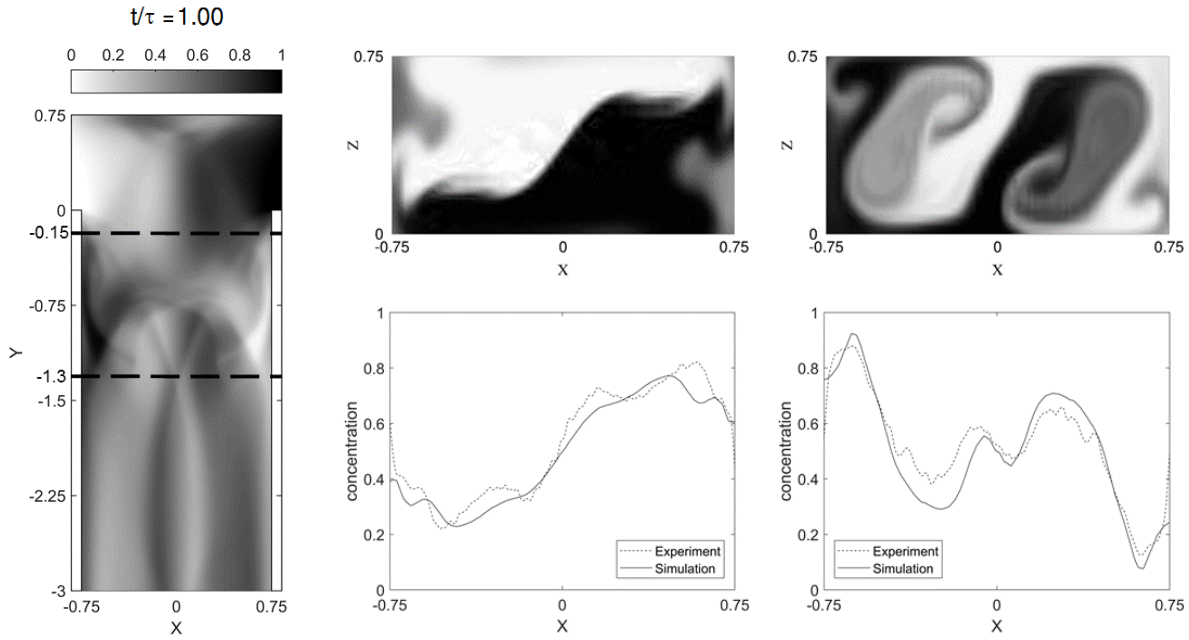
t/τ =1.00
0 0.2 0.4 0.6 0.8 1
0.75
0
-0.15
-0.75
-1.3
-1.5
-2.25
-3
Y
-0.75 0 0.75
X
Z
X
concentration
Experiment
Simulation

(f)

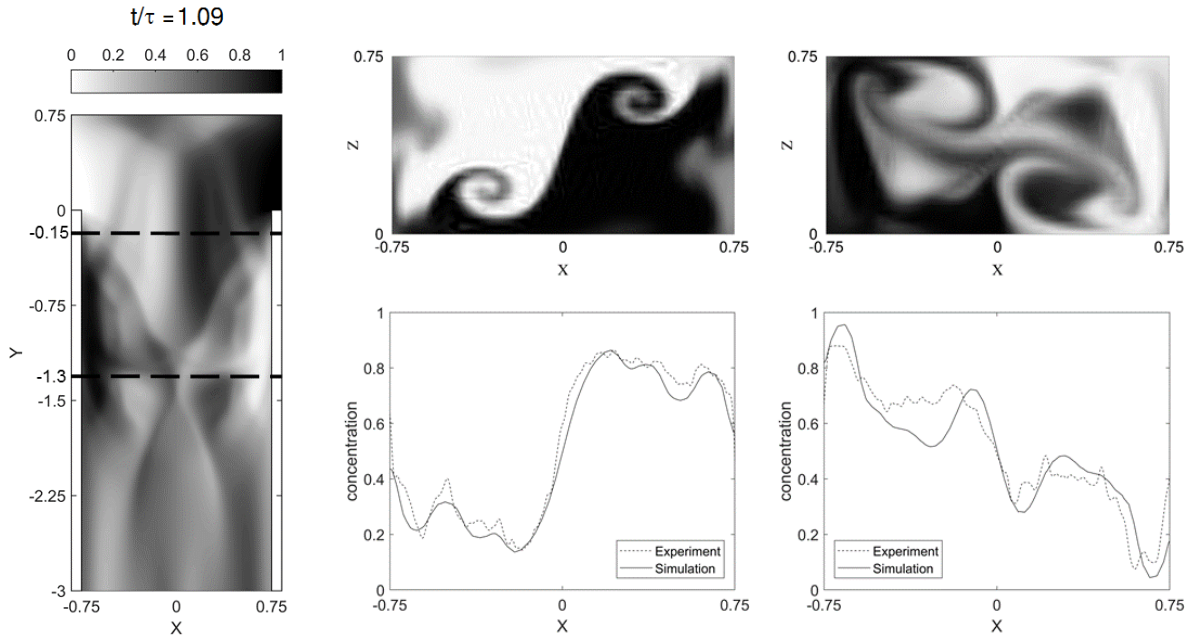

(g)

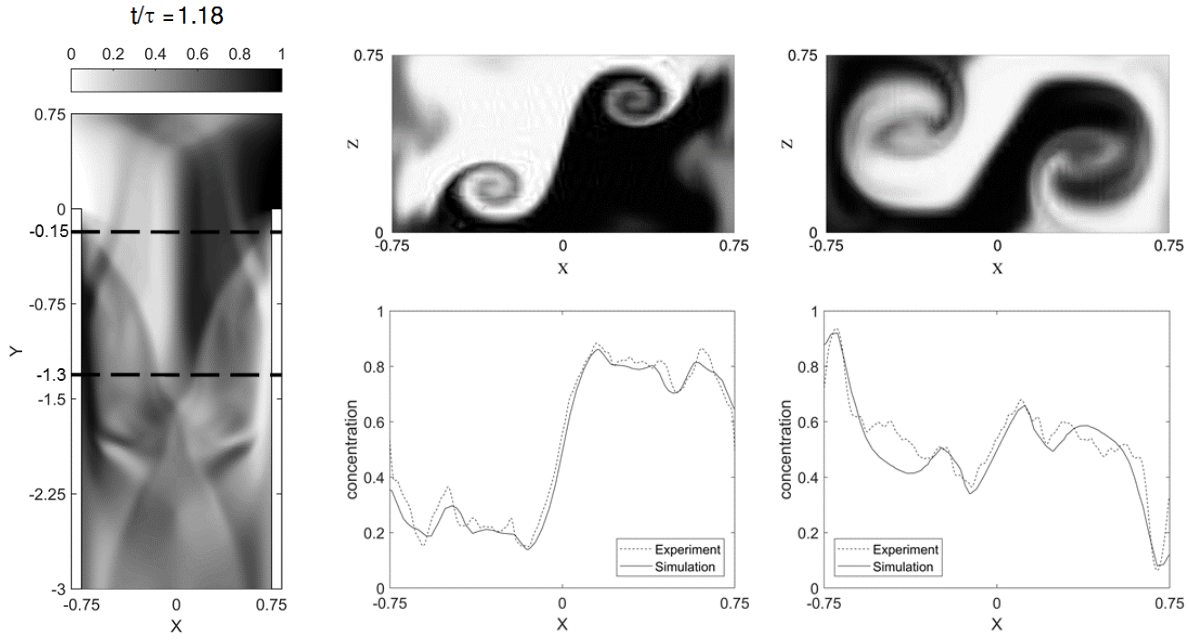

(h)

Figure 3: Dye concentration at $Re = 280$. Distribution of depth-averaged dye concentration predicted using CFD (left). Distribution of dye concentration predicted using CFD at the cross-section $Y = -0.15$ (top-center) and experimental and CFD profiles of depth-averaged dye concentration at $Y = -0.15$ (bottom-center). Distribution of dye concentration predicted using CFD at the cross-section $Y = -1.30$ (top-right) and experimental and CFD profiles of depth-averaged dye concentration at $Y = -1.30$ (bottom-right). Considered instants: (a) $t = 0.27\tau$; (b) $t = 0.64\tau$; (c) $t = 0.73\tau$; (d) $t = 0.82\tau$; (e) $t = 0.91\tau$; (f) $t = 1.00\tau$; (g) $t = 1.09\tau$; (h) $t = 1.18\tau$ (see also the video attached in the supplementary materials).

between the velocity and concentration peaks is lower than 0.1% of the cycle period. Hence, he-depth averaged dye concentration signal can be employed to estimate the characteristic frequency.

Fig. 5 compares experimental and predicted depth-averaged dye concentrations for five cycles at $Re = 280$, showing a total amount of 8 probes at $X = -0.375, -0.185$ and $Y = -0.15, -0.45, -1.3, -2.4$. Here a cycle is computed as the product between the Strouhal number and the non-dimensional time (see the abscissa). Despite the small difference between experimental and predicted St values, i.e. $St = 0.218$ and $St = 0.244$, respectively, the shape of the dye time-signals matches closely.

The same procedure for the analysis of the signals has been repeated for the periodic symmetric regime. In this regime, which was analyzed in detail for the same device in,[23] the two streams are almost segregated and the flow unsteadiness is due to a periodic oscillations of the top parts of the three-dimensional vortical structures, which are also present in the asymmetric regimes and were previously described. Therefore, in this regime, the best probe position is in the confluence region, where the unsteadiness of the flow is more pronounced. Again, the suitability of the depth-averaged concentration to allow the identification of the characteristic frequencies of the flow dynamics, was checked through the comparison between its time behavior and the one of the velocity field (see Fig. 6 for $Re = 450$). As for the analysis previously carried out for $Re = 280$, the difference in the related frequencies is lower than 0.1%. A signature of the small transversal periodic oscillations of the vortical structures in the top region of the mixer may be recognized from the depth-averaged concentration signals. In particular, when they towards negative X values, the stream coming from the right penetrates in the left top part of the mixer (see Fig. 6); the opposite is found when they oscillate towards the right. Then, the experimental and numerical depth-averaged dye concentrations are compared in Fig. 7 for the different cycles and for the two probe locations, i.e. $X = -0.0925, 0$ and $Y = 0.7$. Despite the non-negligible differences in the experimental and numerical Strouhal numbers, i.e. $St = 0.226$ and $St = 0.271$, respectively, the signal

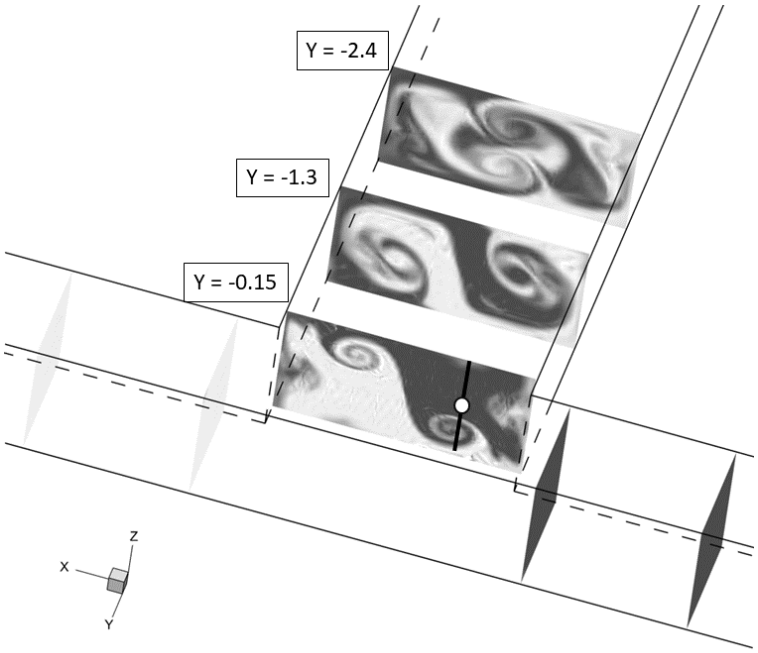

(a)

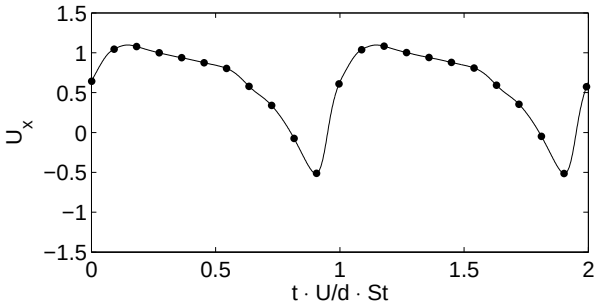

(b)

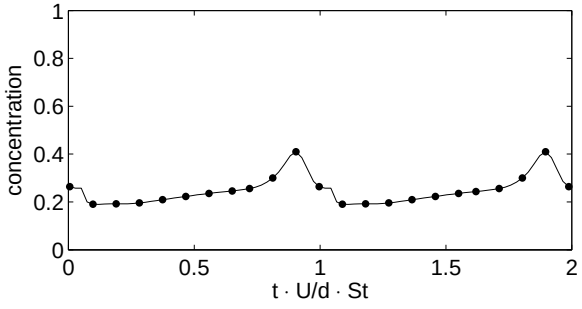

(c)

Figure 4: Numerical simulation at $Re = 280$: (a) position of the considered probes, (b) $x-$velocity signal for the probe positioned at $(X, Y, Z) = (-0.375, -0.15, 0.375)$, (c) depth-averaged dye concentration signal for the probe positioned at $(X, Y) = (-0.375, -0.15)$.

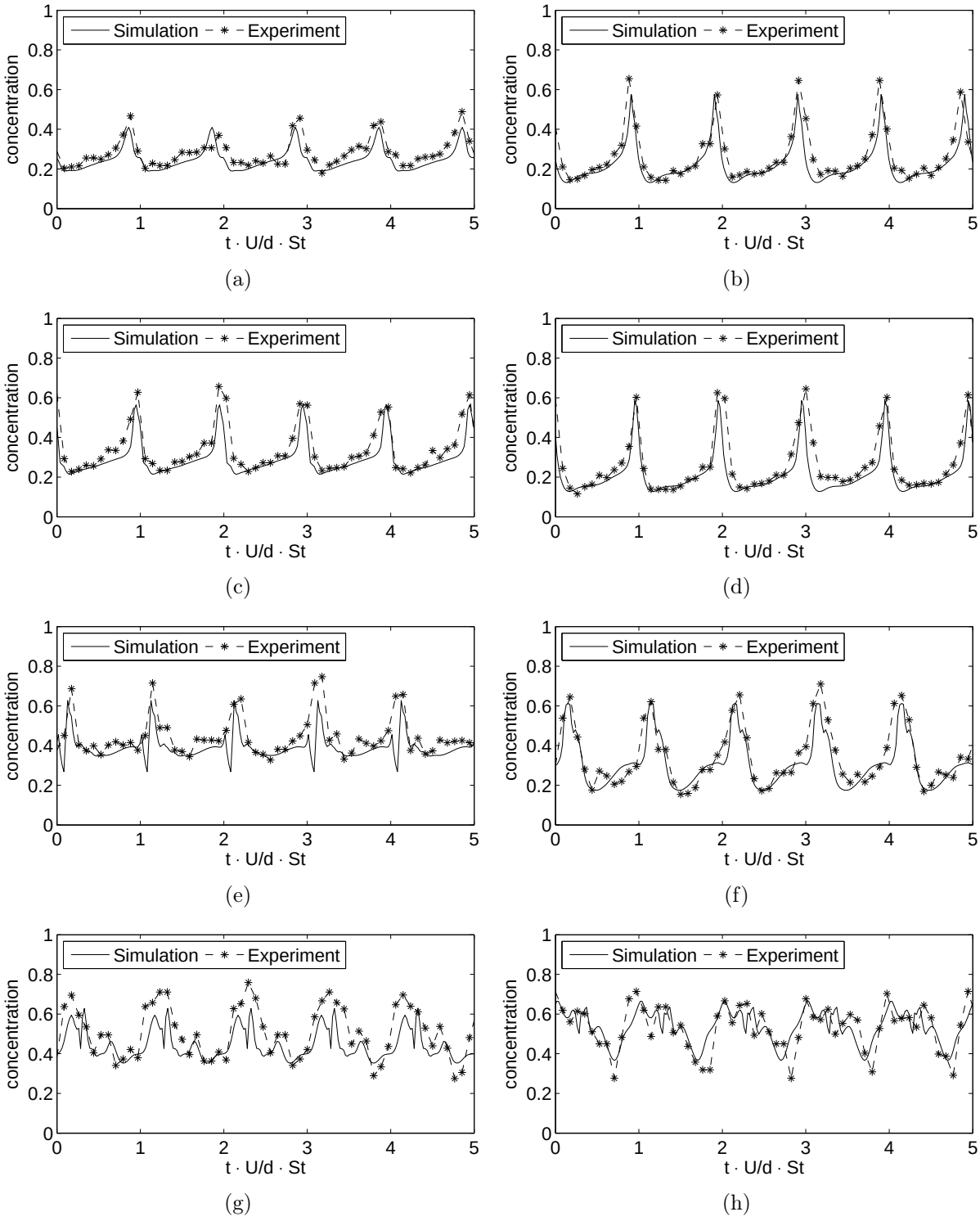

Figure 5: Depth-averaged dye concentration signal at $Re = 280$: comparison between experiments and CFD. Probes positioned at: (a) $(X, Y) = (-0.375, -0.15)$, (b) $(X, Y) = (-0.185, -0.15)$, (c) $(X, Y) = (-0.375, -0.45)$, (d) $(X, Y) = (-0.185, -0.45)$, (e) $(X, Y) = (-0.375, -1.3)$, (f) $(X, Y) = (-0.185, -1.3)$, (g) $(X, Y) = (-0.375, -2.4)$, (h) $(X, Y) = (-0.185, -2.4)$.

profiles match each other closely.

As for the degree of mixing δ_m, defined in eq.(5), only the numerical results are available because for its evaluation the three-dimensional dye and velocity fields are necessary. The mean values of the mixing degree, plus and minus the standard deviation, are reported in Fig. 8(a), showing also the results for the steady regimes. The degree of mixing is evaluated at section $Y = -8$ for the different cases. The asymmetric periodic regime exhibits the maximum value of the degree of mixing. This is due to both the occurrence in the mixing channel of the two co-rotating vortices (as in the engulfment regime) and to the dynamic effect associated with the vorticity blob passage. On the contrary, in the unsteady symmetric regime even lower mixing values than those of the engulfment regime are observed, because of the occurrence of a nearly segregated and symmetric flow topology. The degree of mixing augments in both periodic regimes with the Reynolds number, due to the increase of intensity of the vortical structures.

Strong fluctuations of the degree of mixing characterize the asymmetric time-periodic regime. Such fluctuations are related to the dynamics of the blob of vorticity. This is confirmed by the time-signal of the degree of mixing at $Y = -8$ for $Re = 280$ (see Fig.8(b)). Two high-amplitude fluctuation peaks occur during each cycle when the vorticity blob crosses the considered cross-section; these peaks are followed by a low-amplitude fluctuation. The symmetric regime presents only moderate fluctuations, as the flow unsteadiness mainly affects the top part of the mixer and the interface between the two streams (see Fig.8(c) for $Re = 450$). The double frequency governs the dynamics of the degree of mixing, because the shift of the top part of the vortical structures towards one or the other inlet channel produces the same effect on the mixing degree (see eq. (6)). Thus, the same time behavior of the mixing degree is found for each half period.

The same analyses were repeated for different Re in the range $Re = 235 - 500$. The flow pattern is qualitatively the same within each of the two periodic regimes. The Strouhal numbers calculated for all the experiments and simulations are reported in Fig. 9. Available re-

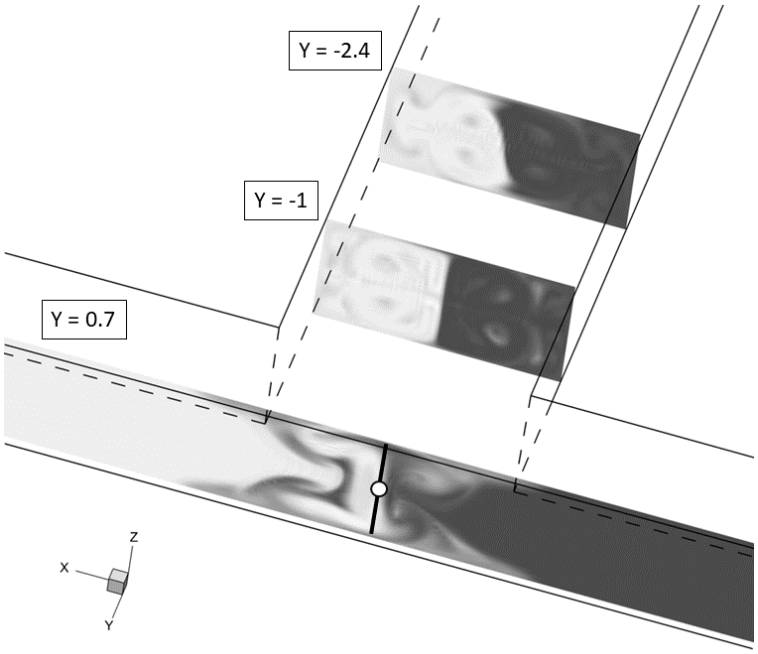

(a)

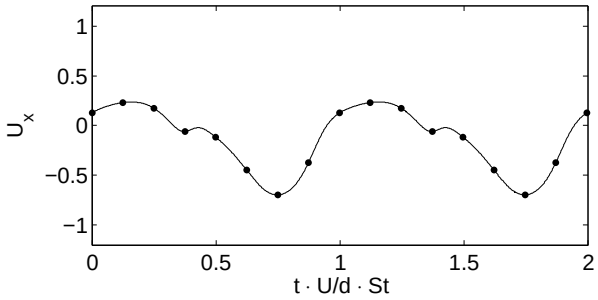

(b)

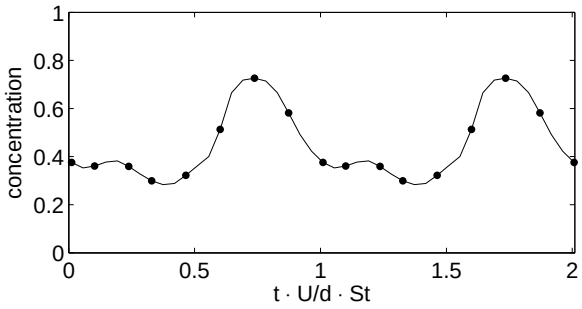

(c)

Figure 6: Numerical simulation at $Re = 450$: (a) position of the considered probes, (b) $x-$velocity signal for the probe positioned at $(X, Y, Z) = (-0.0925, 0.7, 0.375)$, (c) depth-averaged dye concentration signal for the probe positioned at $(X, Y) = (-0.0925, 0.7)$.

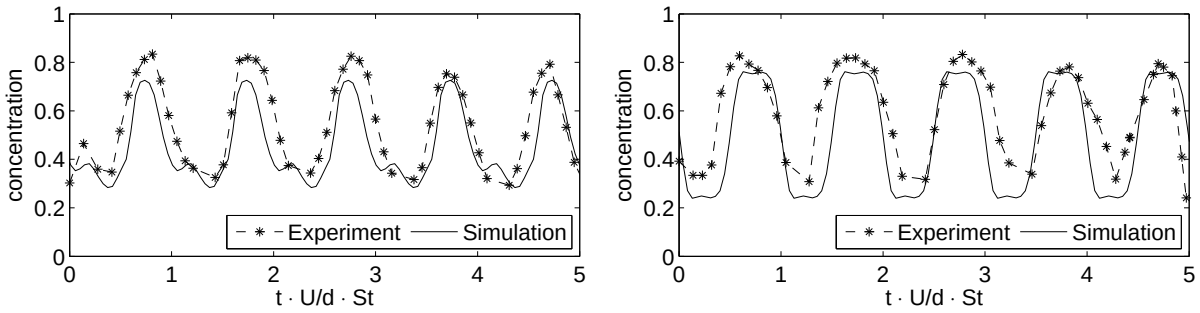

Figure 7: Depth-averaged dye concentration signal at $Re = 450$: comparison between experiments and CFD. Probes positioned at: (a) $(X, Y) = (-0.0925, 0.7)$, (b) $(X, Y) = (0, 0.7)$,

sults from literature[16,29] are also given for comparison. In the experiments, the reported data corresponds to the average value plus and minus the standard error of the Strouhal number of 10 signals of the depth-averaged dye concentration acquired at $(X, Y) = (-0, 185; -0, 15)$. The standard error is evaluated as $err = 2\sigma/\sqrt{n-1}$, where σ is the standard deviation and n the total number of signals. Some discrepancies between experiments and predictions can be noticed, nevertheless they are within the dispersion of data from literature. It can be noticed that both the numerical and experimental St numbers increases monotonically in both asymmetric and symmetric periodic regimes, while a sudden variation of St is observed at the transition between the two periodic regimes.

Characteristic time-scales in the periodic regimes

In the previous Section we found that St augments with the Reynolds number both in the asymmetric and symmetric regimes. Herein we investigate whether proper time-scales can be identified to obtain a Strouhal number that is independent from the Reynolds number in the two periodic regimes. To this aim we investigate more deeply which are the most significant features characterizing the flow dynamics in these regimes.

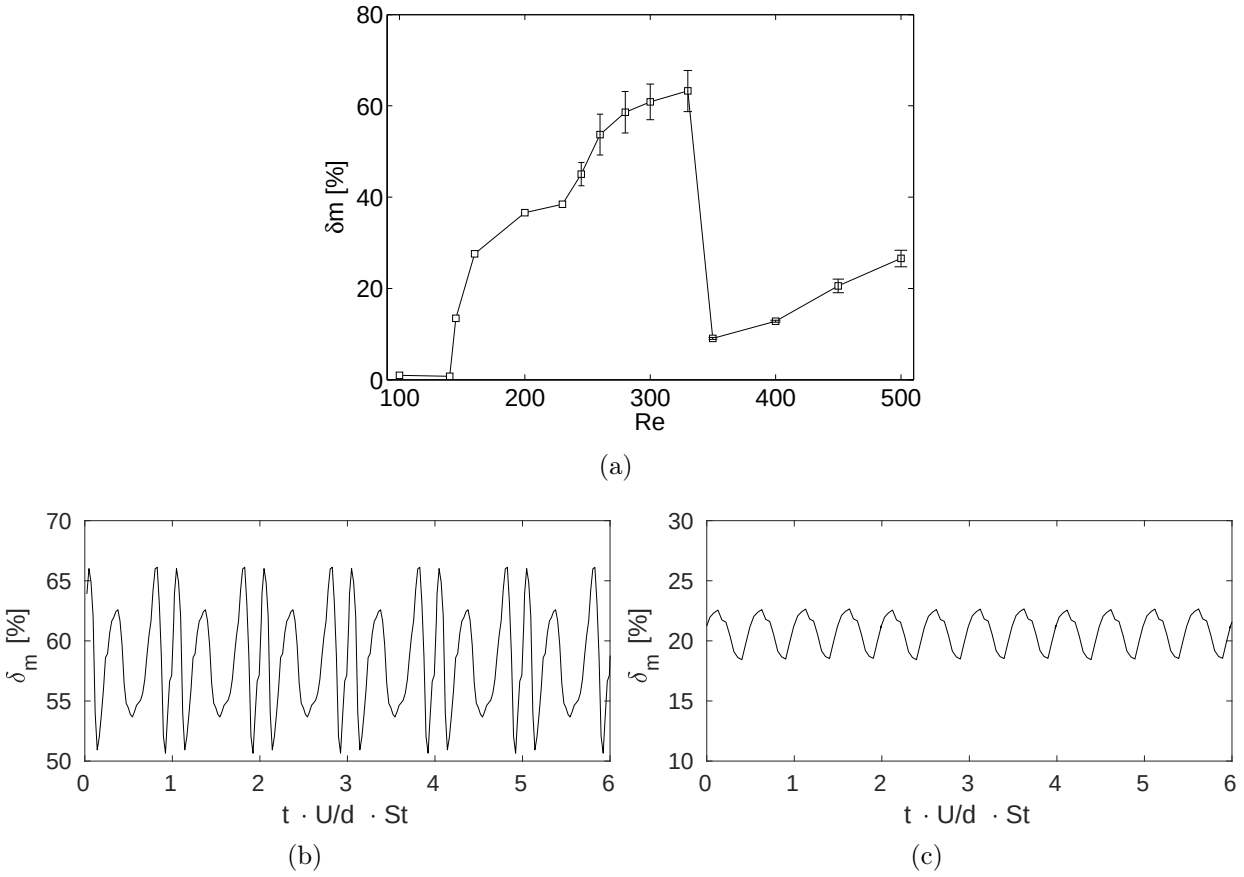

Figure 8: (a) Degree of mixing evaluated at the cross-section $Y = -8$ vs. Reynolds number for different CFD simulations. Time signal of the degree of mixing for 6 cycles at $Re = 280$ (b) and at $Re = 450$ (c).

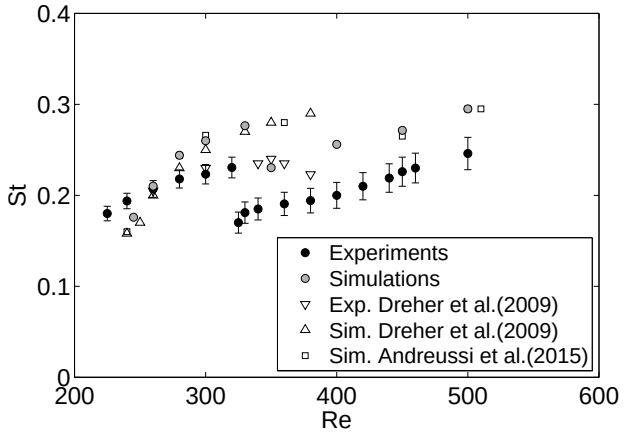

Figure 9: Experimental and numerical Strouhal numbers as a function of the Reynolds numbers.

Asymmetric periodic regime

As described in Sec. 5 and also in,[23,26,29] the cycles of the asymmetric periodic regime are characterized by two main phases: one during which the top parts of the vortical structures become closer and rotate increasing their tilting angle, followed by one in which the two vortical structures merge and a blob of vorticity is convected in the mixing channel. The rotation of the vortical structures is shown for the simulation at $Re = 280$ through the visualization of the isosurfaces of the vortex indicator λ_2 (see[39]) at different times in Fig. 10. During the instants of this rotation the flow patterns (Fig. 11) remain similar to the one previously found for the engulfment regime (e.g. in[23]). The white lines in Fig. 11 indicate the flow region identified as a recirculation according to the λ_2 criterion on the mixer section at $z = H/2$ for different time instants and the non-dimensional pressure fields and the streamlines of the in-plane velocity are also shown in the Figure.

For the considered case, the rotation of the top part of the vortical structures is almost linear in time and goes from $\alpha = 120°$ up to $\alpha = 155°$, as shown in Fig. 12(a) which reports the tilting angle of the top parts of the vortical structures (see Fig. 10). Once reached this latter value of α, the top parts of the two vortical structures merge and rapidly annihilate because they contain vorticity of different sign. The interval in which no data are present corresponds to when the structures disappear after merging and a vorticity blob is shed in the mixing channel. The same behavior is observed for all the considered Reynolds numbers in the asymmetric periodic regime, i.e. $245 \leq Re \leq 330$. It is evident that the maximum and minimum values of the tilting angles and the rotation rate are independent of Re and also the portion of the cycle in which the blob is shed is independent of Re. In particular, the rotation of the top parts of the recirculation regions occurs in the 60% of the whole cycle (e.g. $t \cdot U/d \cdot St \cong 0.1 - 0.7$). Since the rotation angle of the vortex top parts is the same for all Re, but the rotation period is inversely proportional to the cycle frequency, which conversely increases with Re, we can derive that the angular velocity ω_r increases with Re (see Fig. 12(b)). In addition, the Strouhal numbers have an analogous increment with the Re

(see Fig. 12(c), which reports the same numerical results previously shown in Fig. 9 limited to the unsteady asymmetric regime). Consequently, a suitable Strouhal number St_{asymm}, defined as $St_{asymm} = 1/\tau\omega_r$ is independent of Re and the angular velocity ω_r is thus the proper scaling factor in this regime (see Fig. 12(d)). It should be noted that, from a physical point of view, the proposed St_{asymm} is equal to the ratio between the portion of the cycle in which the top part of the vortical structures rotate and the whole cycle period and that this ratio is constant for the considered regime.

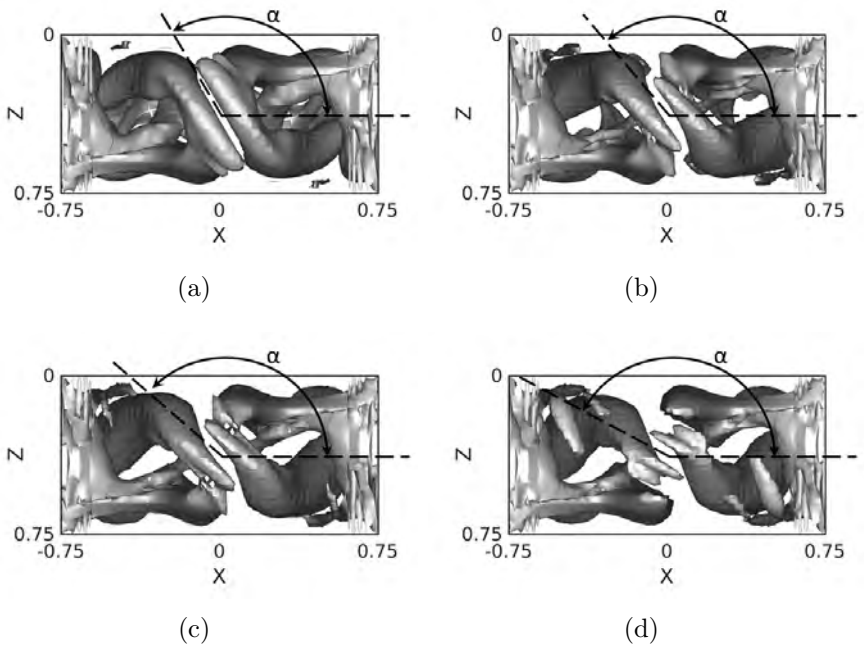

Figure 10: λ_2 isosurface at $Re = 280$ for different instants: (a) $t = 0.10\tau$, (b) $t = 0.28\tau$, (c) $t = 0.46\tau$ and (d) $t = 0.64\tau$.

Symmetric periodic regime

A complete cycle of the symmetric periodic regime is shown for the simulation at $Re = 450$ in Fig. 13, where the isosurfaces of the vortex indicator λ_2 are given for different times at $\tau/4$ of the cycle. Small periodic oscillations in the X direction of the top parts of the 3D vortical structures are evident; their tilting angle changes slightly even though it remains very low, thus not sufficient to break the double mirror symmetry in the mixing channel. The

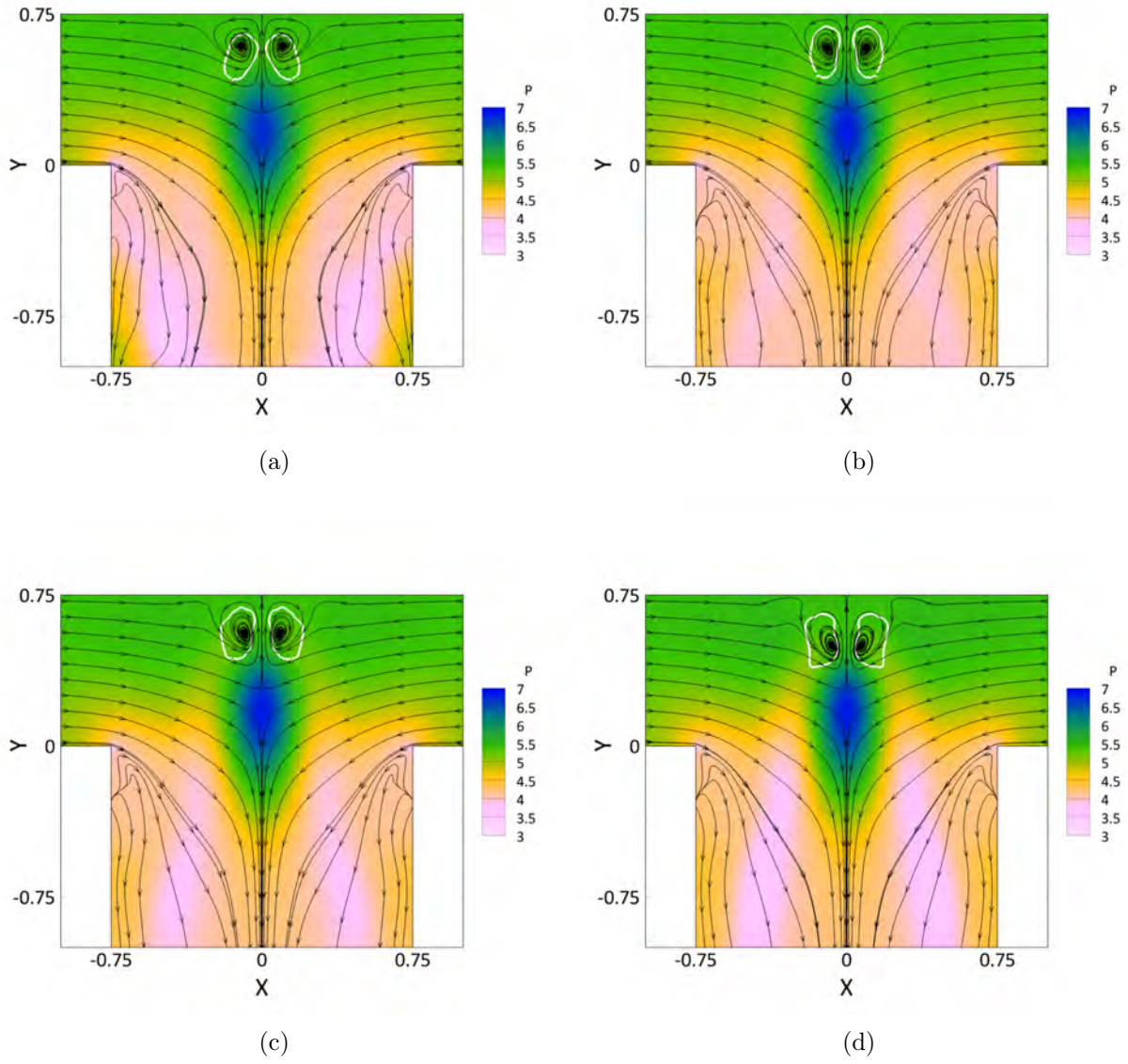

(a) (b)

(c) (d)

Figure 11: Non-dimensional pressure field (color contour) and streamlines (black lines) of the in-plane velocity on the section of the mixer at $z = H/2$ at $Re = 280$ for different instants: (a) $t = 0.10\tau$, (b) $t = 0.28\tau$, (c) $t = 0.46\tau$ and (d) $t = 0.64\tau$. The white lines indicate the flow region identified as a recirculation according to the λ_2 criterion.

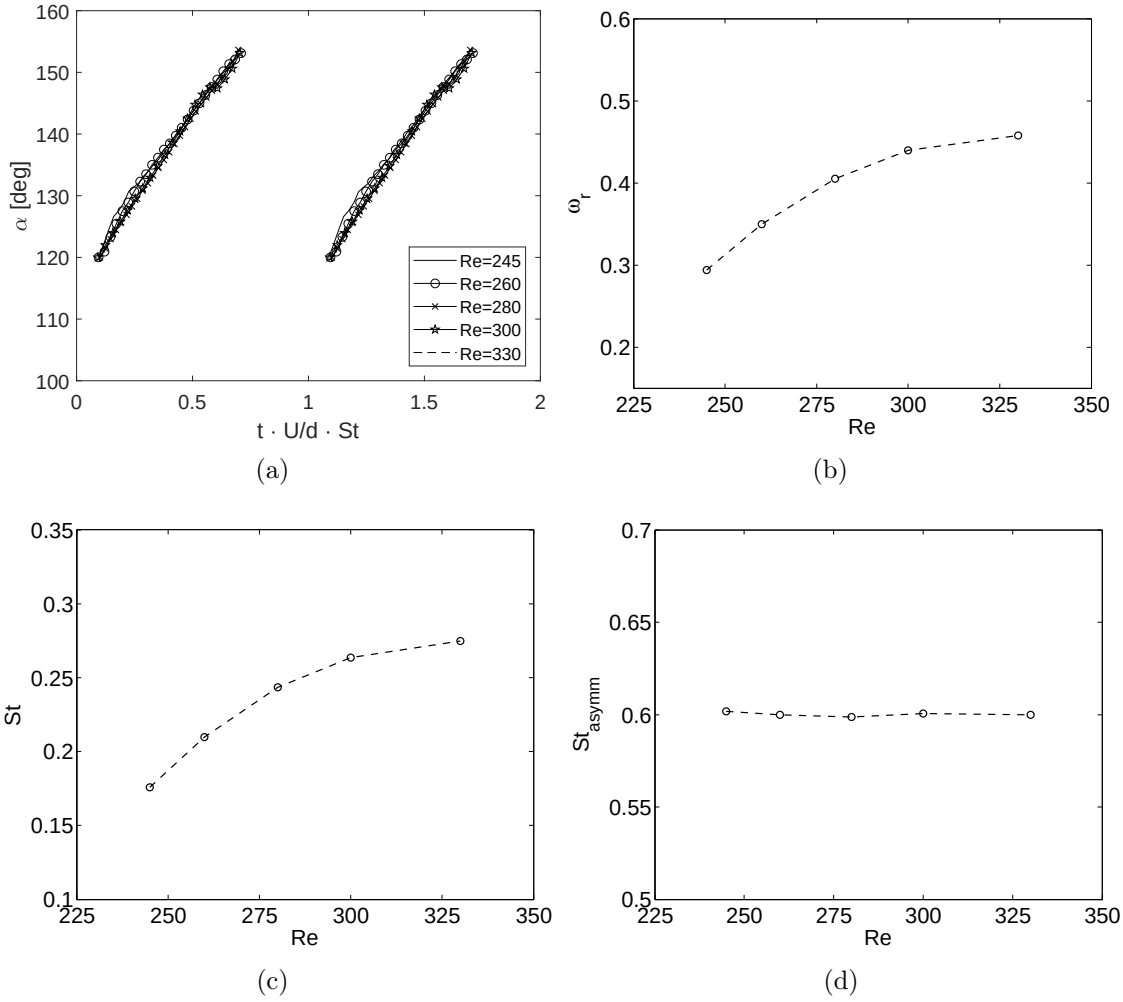

Figure 12: Time behavior of the tilting angle of the recirculation regions for different Reynolds numbers (a). Angular velocity ω_r (b), Strouhal number $St = d/U\tau$ (c) and proposed Strouhal number $St_{asymm} = 1/\tau\omega_r$ (d) for the different Reynolds numbers.

oscillation of the recirculations in the top part of the mixing channel is clearly visible also from the non-dimensional pressure field and in the streamlines of the in-plane velocity shown in Fig. 14. As for Fig. 11, the white lines point out the recirculation regions determined with the λ_2 criterion. The time behavior of the horizontal position of the vortical structures for different Reynolds numbers are compared in Fig. 15(a). The results show that by increasing the Reynolds number the horizontal translation of the top part of the recirculations does not significantly change.

Since the oscillation amplitude x_v is the same for all Re, but the period of the oscillation τ is inversely proportional to the frequency, the mean velocity of the oscillation, $U_v = x_v/\tau$, increases with Re (see Fig. 15(b)). Also the non-dimensional frequency increases with Re (see Fig. 15(c)) and a suitable Strouhal number St_{symm}, defined as $St_{symm} = L/\tau U_v$ (with L being any Reynolds-independent length) is independent of Reynolds (see Fig. 15(d)). Thus, the mean velocity of the oscillation U_v can be considered as the proper scaling factor in this regime.

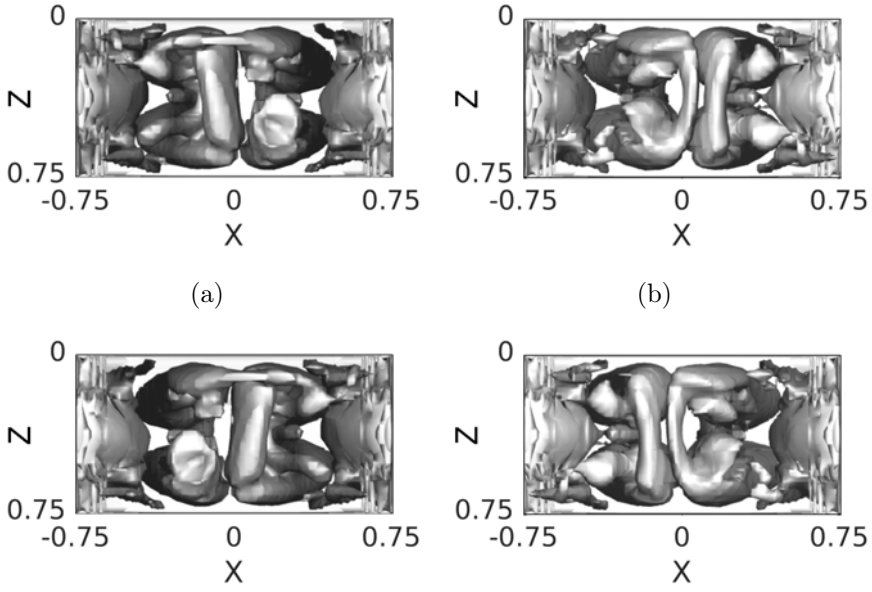

Figure 13: λ_2 isosurface λ_2 at $Re = 450$ for different instants: $t = 0\tau$, (b) $t = 0.25\tau$, (c) $t = 0.50\tau$ and (d) $t = 0.75\tau$.

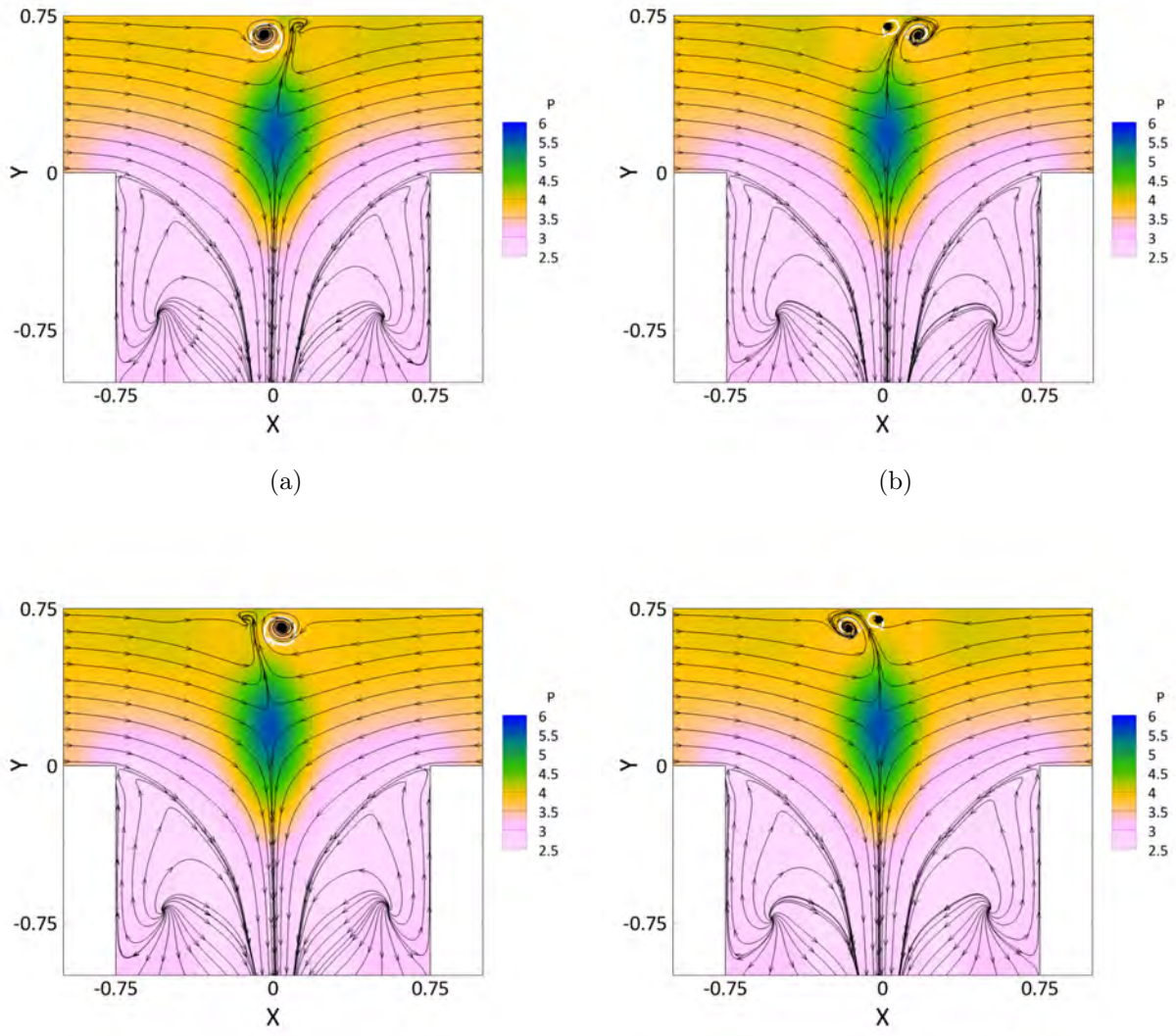

(a) (b)

(c) (d)

Figure 14: Non-dimensional pressure field (color contour) and streamlines (black lines) of the in-plane velocity on the section of the mixer at $z = H/2$ at $Re = 450$ for different instants: (a) $t = 0\tau$, (b) $t = 0.25\tau$, (c) $t = 0.50\tau$ and (d) $t = 0.75\tau$. The white lines indicate the flow region identified as a recirculation according to the λ_2 criterion.

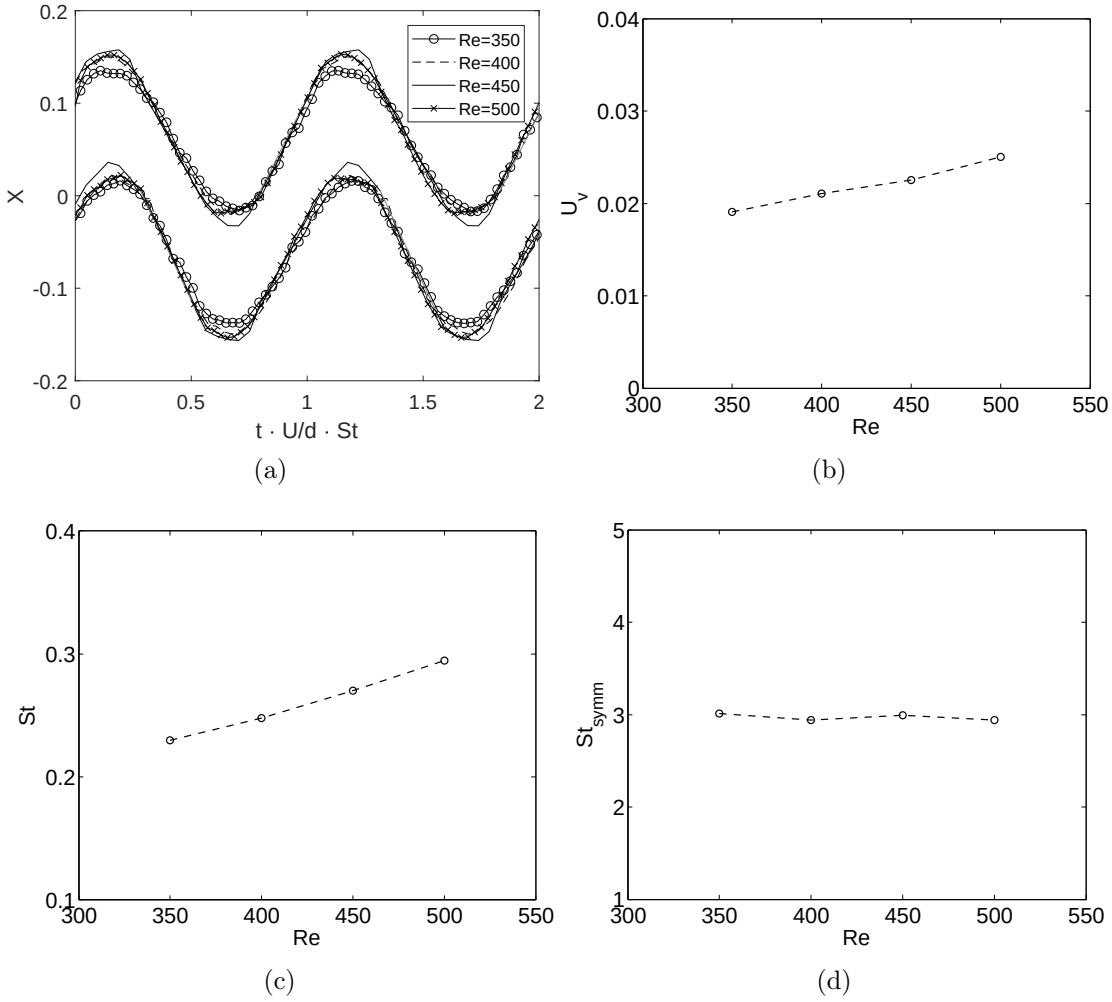

Figure 15: Time behavior of the horizontal position of the recirculation regions for different Reynolds numbers (a). Mean velocity of the oscillation U_v (b) Strouhal number $St = d/U\tau$ (c) and proposed Strouhal number $St_{symm} = L/\tau U_v$ (d) for the different Reynolds numbers.

Conclusions

The time-periodic asymmetric and symmetric regimes, which take place in T-shaped micro-mixers, have been further investigated herein by joint experiments and numerical simulations.

~~In both regimes, the main features of the time periodic cycles have been shown by means of the experimental flow visualizations and of the scalar concentration field available in numerical simulations. Then, thanks to the simultaneous availability of three-dimensional velocity and concentration fields in numerical simulations,~~ It was ascertained that the depth-averaged concentration fields, measured in experiments, can be used to obtain the characteristic frequencies of the flow dynamics. Depth-averaged concentration signals extracted at suitable positions in experiments and simulations were then compared and analyzed. The agreement between experiments and CFD is excellent with $R^2 \geq 0.965$. In the asymmetric regime, the concentration signals recorded in the mixing channel show large peaks each time the vorticity blob, which is periodically shed in this regime, reaches the probe position. Conversely, in the symmetric regime the flow unsteadiness is only due to the periodic oscillating motion of the vortical structures near the top mixer wall; the concentration signals show therefore much less concentrated and pronounced peaks than in the asymmetric regime.

~~The time-averaged degree of mixing, as well as its time fluctuations, have also been computed from numerical simulations as a function of the Reynolds number. As expected, both the time average and the fluctuations of the mixing degree are~~ The time-averaged degree of mixing and its time fluctuation are both significantly larger in the asymmetric regime than in the symmetric regime. This is due to the two co-rotating vortical structures present in the mixing channel, typical of the steady engulfment regime as well, but also to the vorticity blob periodically shed in the mixing channel, which was previously shown to yield large peaks in local passive scalar concentrations. A dramatic decrease of mixing is observed with the onset of the symmetric regime, which is also characterized by much lower fluctuations of δ_m.

~~Finally, the Strouhal number, based on the inlet bulk velocity and hydraulic diameter of the mixing channel, has been computed both in experiments and simulations as a function~~

~~of the Reynolds number and compared to data available in the literature.~~ The agreement between our experimental and numerical Strouhal numbers is not perfect, nevertheless the discrepancies are of the same order of the dispersion of the literature data. In spite of the dispersion, a common feature is that, within both the asymmetric and symmetric regimes, the Strouhal number , based on the inlet bulk velocity and hydraulic diameter of the mixing channel, augments with Re. We tried then to highlight which are the most important dynamical phenomena which influence the characteristic time frequencies and can explain their dependence on the Reynolds number. In both regimes, the characteristic time-scales are linked to the dynamics of the top parts of the 3D vortical structures present in the mixer. The rotation angular velocity is the proper scaling factor of the time-frequency to obtain independency of the Reynolds number in the unsteady asymmetric periodic regime, while the mean lateral displacement velocity can be used in the unsteady symmetric periodic regime together with a geometrical reference length.

A proper quantification of the relevant time frequencies and of the physical phenomena mostly influencing the periodic dynamics, can be useful in practice, for instance, to design active control strategies aimed at promoting mixing by exciting the flow, at the inlet or in proper locations inside the mixer, at the frequencies typical of the asymmetric unsteady regime.

Supporting Information

Video of the experimental flow visualization of the different flow regimes occurring in the T-mixer.

Video of: the distribution of depth-averaged dye concentration predicted using CFD (left); the distribution of dye concentration predicted using CFD at the cross-section $Y = -0.15$ (top-center); the experimental and CFD profiles of depth-averaged dye concentration at

$Y = -0.15$ (bottom-center); the distribution of dye concentration predicted using CFD at the cross-section $Y = -1.30$ (top-right); the experimental and CFD profiles of depth-averaged dye concentration at $Y = -1.30$ (bottom-right).

Acknowledgments

The present work was financed through the "Progetti di Ricerca di Ateneo PRA 2017-2018" funding program by the University of Pisa. The computational resources were made available from CINECA computing center (Bologna, Italy) under the ISCRA program (class B project "MIRE"). We also would like to thank Matteo Antognoli, Tommaso Pannuzi, Deborah Spaltro and Cesare Merello.

References

(1) Van Gerven, T.; Stankiewicz, A. Structure, Energy, Synergy, Time-The Fundamentals of Process Intensification. *Ind. Eng. Chem. Res.* **2009**, *48*, 2465.

(2) Hessel, V.; Löwe, H.; Schönfeld, F. Micromixers-a review on passive and active mixing principles. *Chem. Eng. Sci.* **2005**, *60*, 2479.

(3) Rossetti, I.; Compagnoni, M. Chemical reaction engineering, process design and scale-up issues at the frontier of synthesis: Flow chemistry. *Chem. Eng. J.* **2016**, *296*, 56.

(4) Su, Y.; Lautenschleger, A.; Chen, G.; Kenig, E. Y. A Numerical Study on Liquid Mixing in Multichannel Micromixers. *Ind. Eng. Chem. Res.* **2014**, *53*, 390.

(5) Zhang, W.; Wang, X.; Feng, X.; Yang, C.; Mao, Z.-S. Investigation of Mixing Performance in Passive Micromixers. *Ind. Eng. Chem. Res.* **2016**, *55*, 10036.

(6) Roudgar, M.; Brunazzi, E.; Galletti, C.; Mauri, R. Numerical Study of Split T-Micromixers. *Chem. Eng. Technol.* **2012**, *35*, 1291.

(7) Ortega-Casanova, J. Application of CFD on the optimization by response surface methodology of a micromixing unit and its use as a chemical microreactor. *Chem. Eng. Process.* **2017**, *117*, 18.

(8) Hermann, P.; Timmermann, J.; Hoffmann, M.; SchlÃijter, M.; Hofmann, C.; LÃűb, P.; Ziegenbalg, D. Optimization of a split and recombine micromixer by improved exploitation of secondary flows. *Chemical Engineering Journal* **2018**, *334*, 1996 – 2003.

(9) Ito, Y.; Komori, S. A vibration technique for promoting liquid mixing and reaction in a microchannel. *AIChE J.* **2006**, *52*, 3011.

(10) Sun, C.-L.; Sie, J.-Y. Active mixing in diverging microchannels. *Microfluid. Nanofluid.* **2010**, *8*, 485.

(11) Erkoç, E.; Fonte, C. P.; Dias, M. M.; Lopes, J. C. B.; Santos, R. J. Numerical study of active mixing over a dynamic flow field in a T-jets mixerâĂŤInduction of resonance. *Chem. Eng. Res. Des.* **2016**, *106*, 74.

(12) Bothe, D.; Stemich, C.; Warnecke, H.-J. Computation of scales and quality of mixing in a T-shaped microreactor. *Computers Chemical Engineering* **2008**, *32*, 108 – 114, Process Systems Engineering: Contributions on the State-of-the-Art.

(13) Hoffmann, M.; Schlüter, M.; Räbiger, N. Experimental investigation of liquid-liquid mixing in T-shaped micro-mixers using micro-LIF and micro-PIV. *Chem. Eng. Sci.* **2006**, *61*, 2968.

(14) Bothe, D.; Stemich, C.; Warnecke, H.-J. Fluid mixing in a T-shaped micro-mixer. *Chem. Eng. Sci.* **2006**, *61*, 2950.

(15) Bothe, D.; Stemich, C.; Warnecke, H.-J. In *16th European Symposium on Computer Aided Process Engineering and 9th International Symposium on Process Systems Engi-*

neering; Marquardt, W., Pantelides, C., Eds.; Computer Aided Chemical Engineering; Elsevier, 2006; Vol. 21; pp 351 – 357.

(16) Dreher, S.; Kockmann, N.; Woias, P. Characterization of laminar transient flow regimes and mixing in T-shaped micromixers. *Heat Transfer Eng.* **2009**, *30*, 91.

(17) Soleymani, A.; Yousefi, H.; Turunen, I. Dimensionless number for identification of flow patterns inside a T-micromixer. *Chem. Eng. Sci.* **2008**, *63*, 5291.

(18) Santos, R. J.; Sultan, M. A. State of the Art of Mini/Micro Jet Reactors. *Chem. Eng. Technol.* **2013**, *36(6)*, 937.

(19) Kockmann, N.; Kiefer, T.; Engler, M.; Woias, P. Convective mixing and chemical reactions in microchannels with high flow rates. *Sensors and Actuators B: Chemical* **2006**, *117*, 495.

(20) Hussong, J.; Lindken, R.; Pourquie, M.; Westerweel, J. Numerical Study on the Flow Physics ofÂăaÂăT-Shaped Micro Mixer. IUTAM Symposium on Advances in Micro- and Nanofluidics. Dordrecht, 2009; pp 191–205.

(21) Dreher, S.; Engler, M.; Kockmann, N.; Woias, P. Theoretical and Experimental Investigations of Convective Micromixers and Microreactors for Chemical Reactions. *in: Bockhorn, H., Mewes, D., Peukert, W., Warnecke, H.-J. (Eds.) Micro and Macro Mixing: Analysis, Simulation and Numerical Calculation* **2010**, 325.

(22) Galletti, C.; Brunazzi, E.; Mauri, R. Unsteady mixing of binary liquid mixtures with composition-dependent viscosity. *Chem. Eng. Sci.* **2017**, *164*, 333.

(23) Mariotti, A.; Galletti, C.; Mauri, R.; Salvetti, M. V.; Brunazzi, E. Steady and unsteady regimes in a T-shaped micro-mixer: Synergic experimental and numerical investigation. *Chem. Eng. J.* **2018**, *341*, 414.

(24) Minakov, A. V.; Rudyak, V. Y.; Gavrilov, A. A.; Dekterev, A. A. Mixing in a T-shaped micromixer at moderate Reynolds numbers. *Thermophysics and Aeromechanics* **2012**, *19*, 385.

(25) Minakov, A.; Rudyak, V.; Dekterev, A.; Gavrilov, A. Investigation of slip boundary conditions in the T-shaped microchannel. *Int. J. Heat Fluid Flow* **2013**, *43*, 161.

(26) Fani, A.; Camarri, S.; Salvetti, M. V. Unsteady asymmetric engulfment regime in a T-mixer. *Phys. Fluids* **2014**, *26*.

(27) Thomas, S.; Ameel, T. An experimental investigation of moderate reynolds number flow in a T-Channel. *Exp. Fluids* **2010**, *49*, 1231.

(28) Thomas, S.; Ameel, T.; Guilkey, J. Mixing kinematics of moderate Reynolds number flows in a T-channel. *Phys. Fluids* **2010**, *22*, 1–10.

(29) Andreussi, T.; Galletti, C.; Mauri, R.; Camarri, S.; Salvetti, M. Flow regimes in T-shaped micro-mixers. *Comput. Chem. Eng.* **2015**, *76*, 150.

(30) Ashar Sultan, M.; Fonte, C. P.; Dias, M. M.; Lopes, J. C. B.; Santos, R. J. Experimental study of flow regime and mixing in T-jets mixers. *Chem. Eng. Sci.* **2012**, *73*, 388.

(31) Galletti, C.; Roudgar, M.; Brunazzi, E.; Mauri, R. Effect of inlet conditions on the engulfment pattern in a T-shaped micro-mixer. *Chem. Eng. J.* **2012**, *185-186*, 300.

(32) Mariotti, A.; Galletti, C.; Brunazzi, E.; Salvetti, M. V. Steady flow regimes and mixing performance in arrow-shaped micro-mixers. *Phys. Rev. Fluids* **2019**, *4*, 034201.

(33) Fischer, P. F.; Lottes, J. W.; Kerkemeier, S. G. nek5000 Web page. *Web page: http://nek5000. mcs. anl. gov* **2008**,

(34) Salvetti, M.; Mariotti, A.; Galletti, C.; Brunazzi, E. Steady and unsteady regimes in a T-shaped micro-mixer: Synergic experimental and numerical investigation. *in Proceedings of the ASME 2018 5th Joint US-European Fluids Engineering Division Summer*

Meeting, FEDSM2018 July 15-20, 2018, Montreal, Quebec, Canada, Publisher: American Society of Mechanical Engineers, Fluids Engineering Division, Code 141102 **2018**, *3*.

(35) Galletti, C.; Mariotti, A.; Siconolfi, L.; Mauri, R.; Brunazzi, E. Numerical investigation of flow regimes in T-shaped micromixers: benchmark between finite volume and spectral element methods. *Can. J. Chem. Eng.* **2019**, *97*, 528.

(36) Poole, R. J.; Alfateh, M.; Gauntlett, A. P. Bifurcation in a T-channel junction: Effects of aspect ratio and shear-thinning. *Chem. Eng. Sci.* **2013**, *104*, 839.

(37) Galletti, C.; Arcolini, G.; Brunazzi, E.; Mauri, R. Mixing of binary fluids with composition-dependent viscosity in a T-shaped micro-device. *Chem. Eng. Sci.* **2015**, *123*, 300.

(38) Danckwerts, P. V. The Definition and Measurement of Some Characteristics of Mixtures. *Appl. Sci. Res., Sect. A* **1952**, *3(4)*, 279.

(39) Jeong, J.; Hussain, F. On the identification of a vortex. *J. Fluid Mech.* **1995**, *285*, 69.